REVISION 003

STABILITY OF MAGNESITE IN THE PRESENCE OF HYDROUS FLUIDS UP TO 12 GPA: INSIGHTS INTO SUBDUCTION ZONE PROCESSES AND CARBON CYCLING IN THE EARTH'S MANTLE

Word count: 7226 words (revised manuscript: abstract included, without acknowledgment, references and captions)

Melanie J. Sieber[1,2*], Hans Josef Reichmann[1], Robert Farla[3], Monika Koch-Müller[1]

[1] GFZ German Research Centre for Geosciences, Telegrafenberg, 14473 Potsdam, Germany

[2] present address: University of Potsdam, Institute for Geosciences, Karl-Liebknecht-Strasse 24-25, D-14467 Potsdam, Germany

[3] Deutsches Elektronen-Synchrotron DESY, Notkestraße 85, 22607 Hamburg, Germany

*corresponding author: E-mail address: melanie.sieber@uni-potsdam.de

AUTHORS CONTRIBUTION STATEMENT

MJS performed the experiments and analysis, evaluated the data and wrote the manuscript.

HJR and MKM designed the research proposal, contributed to the discussion of the results and manuscript preparation.

HJR, RF and MKM helped performing in situ experiments and acquisition of EDXRD data

All authors approved the (revised) version of the manuscript to be submitted to American Mineralogist.

ABSTRACT

Understanding the stability of magnesite in the presence of a hydrous fluid in the Earth's upper mantle is crucial for modelling the carbon budget and cycle in the deep Earth.

This study elucidates the behavior of magnesite in the presence of hydrous fluids. We examined the brucite-magnesite ($Mg(OH)_2$-$MgCO_3$) system between 1 and 12 GPa by using synchrotron in situ energy dispersive X-ray diffraction experiments combined with textural observations from quenched experiments employing the falling sphere method. By subjecting magnesite to varying pressure-temperature conditions with controlled fluid proportion, we determined the stability limits of magnesite in the presence of a fluid and periclase.

The observed liquidus provides insights into the fate of magnesite-bearing rocks in subduction zones. Our findings show that magnesite remains stable under typical subduction zone gradients even when infiltrated by hydrous fluids released from dehydration reactions during subduction. We conclude that magnesite can be subducted down to and beyond sub-arc depths. Consequently, our results have important implications for the carbon budget of the Earth's mantle and its role in regulating atmospheric CO_2 levels over geological timescales.

KEYWORDS

- Deep Carbon Cycle
- Brucite dehydration
- Magnesite Melting
- EDXRD

INTRODUCTION

The fates of carbon and hydrogen in the mantle are intimately linked to each other. For instance, the release of $CO_{2,aq}$ from carbonaceous lithologies in the slabs during subduction is enhanced by dehydration reactions, because water acts as catalyst and solvent in decarbonation and dissolution reactions (summarized in Galvez and Pubellier 2019). With increasing water activity, the solidus of carbonate-bearing rocks is drastically reduced promoting the formation of carbonate melts (Wyllie and Tuttle 1960; Poli 2015; Poli et al.

2009). Thus, infiltration of aqueous fluids (e.g. released in dehydration reactions) into slab sediments can produce a carbonate-bearing fluid/melt. The extent to which these processes operate is controversial (Kelemen and Manning 2015; Orcutt et al. 2019). Due to the breakdown of dolomite with increasing pressure, magnesite ($MgCO_3$) is the most dominant carbonate phase in the CO_2-peridotite system above ~4 GPa (Falloon and Green 1989; Dasgupta and Hirschmann 2006; Dasgupta et al. 2004; Shen et al. 2018) and plays an important role in the cycle of oxidized carbon into the deep Earth. However, to date, the stability of magnesite in the presence of a H_2O-bearing fluid is still poorly constrained.

Carbonates in the upper mantle are nominally anhydrous, meaning their crystal structure does not incorporate H_2O, and their stability has been studied intensively (see Shatskiy et al. 2015 and references therein). In the (dry) MgO-CO_2 system, magnesite dissociates up to 2.3 GPa and 1550 °C, where magnesite begins to melt incongruently forming periclase and carbonate liquid (Huang and Wyllie 1976; Irving and Wyllie 1975). Earlier studies reported congruent melting of magnesite at pressures ≥2.7 GPa (Huang and Wyllie 1976; Shatskiy et al. 2016; Katsura and Ito 1990). Sieber et al. (2022) recently revised the melting reaction, demonstrating incongruent melting for magnesite in the anhydrous system at 6 and 9 GPa.

A better investigation of the stability of magnesite in the presence of a free fluid phase is needed, because only a marginally lower liquidus in the water bearing system (1700-1750 °C) compared to anhydrous conditions (1750-1800 °C) was obtained from experiments on hydromagnesite at 6 GPa employing the falling sphere technique in ex situ experiments (Müller et al. 2017). Compared to silicate-bearing system, such a small reduction of the liquidus temperature by H_2O is surprising (e.g. Green et al. 2014). Interpretation of the equilibrium assemblage from quenched experiments based on crystal sizes and textural features is problematic due to the reactivity of the quenched vapors and solids (Walter et al. 1962). For instance, quenched periclase (MgO) reacts with a H_2O-fluid at high pressure to

brucite ($Mg(OH)_2$) (Della Roy and Roy 1957) and with a CO_2-H_2O-fluid to magnesite, brucite, and/or nesquehonite (Walter et al. 1962). Therefore, in situ X-ray diffraction investigations of the melting conditions of magnesite in the presence of an aqueous fluid are strongly needed, because until now melting conditions and phase equilibria are only available from quenched experiments.

We investigate the stability of magnesite in the presence of a hydrous fluid under mantle conditions between 1 and 12 GPa carrying out synchrotron in situ energy dispersive X-ray diffraction experiments and quenched experiments employing the falling sphere technique. Our study confirms the previously published dehydration and melting curves of brucite (Fukui et al. 2005; Johnson and Walker 1993) and determines the pressure and temperature conditions at which magnesite breaks down in the presence of periclase and a free fluid phase.

EXPERIMENTAL AND ANALYTICAL METHODS

Experimental strategy and starting material

By subjecting magnesite to varying pressure-temperature conditions under controlled fluid proportion, we elucidate the breakdown and liquidus of magnesite coexisting with hydrous fluids. High pressure and temperature experiments were performed in large volume presses utilizing either in situ energy dispersive X-ray diffraction (EDXRD) or the falling sphere technique to determine the reactions in the brucite-magnesite system between 1 to 12 GPa. In both experimental approaches the magnesite/fluid-ratio was kept constant by using a mixture of natural magnesite powder ($Mg_{9.9}Fe_{0.1}Ca_{0.03}(CO_3)_{10}$ from Brumado, Brazil) and 16 wt% laboratory-grade brucite as starting material. At 0.4 GPa, the eutectic composition of the brucite-magnesite system is at ~2 wt% brucite (Walter et al. 1962). The starting composition

was chosen to establish a constant amount of ~5 wt% H_2O in the capsule after dehydration of brucite during the heating paths, e.g. at 3.6 GPa and ~1000 °C (Johnson and Walker 1993; Okada et al. 2002; Fukui et al. 2005). Further, by adding 16 wt% brucite to the starting material, sufficient periclase (11 wt%) is formed in the dehydration reaction to be detectable with EDXRD. Periclase (MgO) served as pressure marker inside the capsule of the in situ experiments. Starting mixtures were ground in acetone for ~0.5 h and dried at ~120 °C for several days before being loaded into the capsules.

High pressure experiments

The falling sphere method was applied in a Walker style multi-anvil apparatus at the German Research Centre for Geosciences (GFZ) and in offline experiments using the 'Aster-15' 3 x 5 MN six-ram multi-anvil press at the P61B Large Volume Press (LVP) end-station at the Deutsches Elektronen-Synchrotron (DESY). Details of the multi-anvil press at GFZ are reported in Deon et al. 2011. An 14/8 assembly with double stepped graphite heater was used in the Walker multi-anvil press (GFZ) and an 14/8 assembly with Re-heater in the offline experiments in the Aster-15 LVP (for technical drawings used in the offline experiments see Sieber et al. 2022). Inside the capsules, a Pt-sphere was placed at the top of the starting mixtures but well below the lid. The sample was brought to the target pressure (*P*) and temperature (*T*) for <30 min before being quenched. The location of the Pt-sphere after the experiment and/or the texture of the product after the run was used as melting criterion. If the Pt-sphere is located at the bottom of the capsule, the amount of melt formed is sufficient to allow the sphere to move through the capsule. If the crystal shape of brucite grains was dendritic, they were interpreted as having been formed by quenching from a MgO-rich aqueous fluid/liquid.

In situ EDXRD in the Aster-15 was used to monitor changes in the mineral assemblage of the start material as a function of *PT*. Using EDXRD the onset of melting is indicated by rapid

changes in the peak intensity of solids as a function of heating and this approach has been shown to be very useful to precisely determine the onset of melting (Andrault et al. 2006). Details on the operation of the Aster-15 LVP at the P61B end-station are reported in Farla et al. (2022). One additional 'dry' in situ experiment was performed at ~6 GPa without the addition of brucite. This demonstrates the applicability of the experimental approach and allows comparison between in situ experiments and published (offline) experiments employing the falling sphere technique (Müller et al. 2017; Shatskiy et al. 2018).

Each starting material was loaded in a single crystal diamond cylinder enclosed on top and bottom by Pt-lids (Figure 1) - similar to the design described in Yamada et al. (2007). The diamond cylinder is X-ray transparent and inert to carbonatitic melts. The ductile behavior of platinum enclosed and sealed the diamond cylinder under compression and upon heating. For in situ experiments, a 14/8-assembly with either graphite or Re-foil as resistivity heater was used. Two holes were drilled into the Re-foil for better X-ray transmission and the material of the outer sleeve (ZrO_2) was replaced by MgO (Figure 1). The sample was brought to the target pressure and then heated stepwise.

Temperature was monitored in all experiments and over the entire run duration with a Type C thermocouple (WRe5%-WRe26%-wires). In case of thermocouple failure, the temperature was estimated from electrical power versus temperature calibrations of identical cell assemblies. The temperature gradient from the thermocouple to the center of the sample is expected to be about 30 °C using Re-heater, according to cell-assembly heating simulations (Hernlund et al. 2006). The temperature gradient is expected to be reduced when using double stepped graphite as heater. Since diamond, which is used as the capsule material, is an excellent thermal conductor we expect a negligible thermal gradient in the sample.

An overview of the performed experiments is provided in Table 1.

Figure 1

Table 1

Analytical techniques

Time-resolved EDXRD measurements and radiography images under high *PT* conditionswere collected at the P61.B end-station (DESY). Two EDXRD systems each consisting of a Ge solid-state detector with a 4096 multichannel analyzer and for radiographic imaging an X-ray microscope with sCMOS camera and a GGG:Eu scintillator (40 µm) are available. The size of the X-ray beam was 50 x 500 µm and 50 x 300 µm for measurements of the sample and periclase, respectively (Figure 1). The exposure time for EDXRD measurements ranged between 300 to 400 s at the sample position and was 200 s for periclase. The diffraction patterns were collected at a fixed 2Θ angle of ~5° and, in experiments with a run number ≥153, also at ~3° using a second detector. During EDXRD measurements the entire LVP was oscillated between -2.5 deg and +2.5 deg.

At the target pressure, the sample was heated by 50-200 °C steps until ~1000 °C was reached and then heated in intervals of +25 °C. EDXRD spectra of the sample were collected at each heating step for phase identification. Our criterion for an unambiguous identification of a mineral phase was the occurrence of at least two reflections that can be indexed by the mineral. Exceptions are indicated in the results. Changes in the mineral assemblage during heating were confirmed in a second EDXRD measurement at a different position in the sample. Heating to higher temperatures continued until all reflections of the samples disappeared in the EDXRD spectra, or until no further change in the mineral assemblage was expected. Afterwards the sample was cooled down gradually.

Pressure was calculated from the positions of the periclase reflections using the pressure-volume-temperature equation of state of Tange et al. (2009). Between 900 and 1100 °C, periclase formed in the sample due to the incongruent breakdown of brucite. This enables comparison of the pressure obtained from the periclase reflections inside the diamond sleeve with the pressure obtained from periclase reflections of the assembly parts (outside the

diamond sleeve). Within the uncertainty, the pressure inside and outside of the diamond sleeves are equal at these high temperatures (Figure S1 in the supplementary information), confirming that above 1000 °C diamond softens sufficiently to equalise the pressure inside and outside of the diamond cylinder. The periclase pressure sensor was measured continuously during heating and over the whole run duration.

Capsules recovered from the offline experiments were mounted, polished and carbon-coated for Scanning Electron Microscopy (SEM) at the University of Potsdam. The post-run phases and textures in samples extracted from the in situ experiments were investigated with a FEI Quanta 3D Dual Beam SEM at the Potsdam Imaging and Spectral Analysis (PISA) Facility at the GFZ. Raman spectroscopy (HORIBA Jobin Yvon LabRAM HR 800) was used at the University of Potsdam for phase identification. Raman spectra over a spectral range of 100-2000 and 3000-4000 cm^{-1} were accumulated over 50 s using an Nd:YAG (532 nm) laser with a 50× objective lens and a 300 grating.

RESULTS

Falling sphere experiments: texture and position of Pt-sphere

In the falling sphere experiments, the Pt-sphere's descent from the top to the bottom of the capsule under high *PT* conditions indicates the formation of a sufficient amount of melt, enabling the sphere's movement within the capsule. However, the production of small amounts of melt may prevent the sphere from reaching the bottom. Another indicator of melt occurrence under high *PT* is the texture of quenched phases. In the following we will use both, the position of the Pt-sphere and the texture, as indicators for melting.

In run 87 performed at 10.8 GPa and 1800 °C, the Pt-sphere is found at the bottom of the capsule. In contrast, in run 88 performed at the same pressure but lower temperature (~1485 °C), the Pt-sphere remains at the top, while magnesite, periclase and brucite exist. Therefore, the liquidus at 10.8 GPa lies somewhere between 1485 °C and 1800 °C.

The same pair of experiments was conducted at 6 GPa. At 1300 °C (run 120), the sphere remains at the top, and the presence of periclase suggests the dehydration of brucite. An hourglass texture is observed (Figure 2a), likely resulting from a thermal gradient in the capsule. Magnesite + periclase occur in the colder region, while brucite + periclase along with significant pore space exist in the hotter region of the capsule. This hourglass texture is commonly observed in cases involving thermal gradients as seen in melting experiments with the same experimental setup (Sieber et al. 2020; Sieber et al. 2022), experiments involving large amount of fluids (e.g. Deon et al. 2011) and experiments on brucite dehydration (Johnson and Walker 1993). Irregularly shaped periclase crystals (5-25 µm) are found next to magnesite, while smaller periclase grains (<5 µm) exist less frequently near dendritic brucite grains. The dehydration of brucite produces periclase + fluid (see discussion), and the fluid diffuses toward the hottest regions of the capsule, while MgO diffuses along the periclase solubility and/or due to thermophoresis (Soret effect) towards the colder regions (Johnson and Walker 1993). Consequently, periclase grains accumulate in the colder regions, surrounded by magnesite, while brucite in the warmer regions may result from a kinetically fast back-reaction (hydration) of periclase with the fluid after quenching. This also explains the lower abundances and smaller grain size of periclase in the hotter region compared to periclase in the colder regions (Johnson and Walker 1993).

At 1760 °C (run 121), the sphere remained at the top, but the texture of elongated magnesite grains and dendritic brucite crystals indicates the presence of a melt (Figure 2b). Periclase crystals are found at the bottom of the capsule, indicating their crystallization in the lower

temperature region, a common phenomenon for subliquidus phases (Fukui et al. 2005; Sieber et al. 2020; Sieber et al. 2022; Inoue 1994). The dendritic texture of brucite crystals in run 121 is attributed to quenching from a MgO-H_2O-bearing melt. Thus, the textural observations imply that at 6 GPa the liquidus is surpassed at 1760 °C, despite the Pt-sphere remaining at the top of the capsule (Figure 2b) likely because of frictional forces.

Figure 2

Although such texture observations are helpful in determining whether melting has occurred or not, determining the melting temperature requires many runs to narrow down the melting temperature. Thus, in situ experiments that allow direct observation of phase stability are advantageous.

In situ experiments: phase assemblage

The mineral phases present in the starting material (magnesite + brucite or magnesite in the dry experiment run 156) were identified though EDXRD at both ambient condition and high pressure (representative X-ray diffraction profiles are shown in Figure 3). In run 130, magnesite and brucite were identified under ambient conditions, while only the (110) line of brucite remained visible at high pressure before heating.

At the target pressure, the samples were gradually heated to monitor changes in the mineral phases. In the hydrous system, the first change observed with increasing temperature is the transition from magnesite + brucite to magnesite + periclase. This phase transition is clearly defined by the disappearance of brucite reflections and appearance of periclase reflections (Figure 3). The identification of periclase by EDXRD marks an upper bound since the amount of formed periclase must be sufficient to be detectable. Brucite is stable up to 850 °C at 1.8 GPa (run 158) and up to 1100 °C at 3.4 GPa (run 157). Above ~4 GPa, brucite exists up to ~1150 °C. Note that only the (110) line of brucite indicates its presence in run 130 for

temperatures between ~1000 and ~1100 °C and in run 153 up to ~1000 °C. Periclase is observed in all experiments, expect for run 127, where its absence in the EDXRD spectra may be attributed to poor packing of the starting powder or the loss of some fluid after brucite dehydration. Small amounts of periclase crystals were observed in the post-run sample by SEM for all experiments.

The second change in mineral assemblage observed with increasing temperature is the disappearance of magnesite. Between 1 and 6 GPa, the stability of magnesite extends to higher temperature with increasing pressure. For instance, magnesite remains stable up to ~1200 °C at 1.6 GPa (run 158), to ~1400 °C at 3.5 GPa (run 157) and ~1500 °C at 4.7 GPa (run 153). Between 6 and 9 GPa, magnesite occurs up to ~1650 °C. Magnesite disappears with further temperature increase.

At pressures below 6 GPa, periclase remains stable even at the highest investigated temperatures (Figure 3a). At 6.6 and 8.3 GPa, and a temperature above ~1690 °C, all mineral reflections disappear from the EDXRD spectra (Figure 3b, 3c).

Figure 3

In the anhydrous experiment (run 156) performed at ~6 GPa, magnesite remains stable up to 1725 °C. At slightly higher temperature (1750 °C), periclase forms as a result of the breakdown of magnesite.

During cooling, the reversed phase transformation occurs at significant lower temperature due to hysteresis. The post-run samples recovered from the in situ experiments mainly contain magnesite, along with some periclase and brucite (Figure 2c,d). The presence of brucite or an OH-bearing phase in the post-run assemblages verifies that the capsules

remained sealed throughout the experiment, except for runs 128 and 131, which were excluded from the analysis (Table 1). At the rim to the diamond cylinder, small amounts of graphite were observed in the post-run assemblage of run 127, potentially originating from the laser cutting of the diamonds. If graphite had formed during the experiments, we would expect to find it in more samples and for it to be randomly distributed within the sample. These features are not observed.

DISCUSSION

Brucite – out and periclase in

The EDXRD data reveal the formation of periclase at the expense of brucite. The reported *PT* conditions at which brucite decomposes and periclase forms align well with their stability fields determined by techniques such as differential thermal analysis, quenched experiments (Johnson and Walker 1993), in situ X-ray observations (Okada et al. 2002) and a combination of quenched and in situ experiments with thermodynamic calculations (Fukui et al. 2005) (Figure 4b). However, one exception is run 130 (6.6 GPa) where periclase occurs at a temperature which is ~100 °C lower than expected based on the aforementioned previous studies.

The decomposition mechanism of brucite depends on the pressure (Fukui et al. 2005; Okada et al. 2002; Johnson and Walker 1993). Up to at least 4 GPa, brucite dehydrates. As pressure increases, the decomposition mechanism of brucite changes due to the enhanced solubility of MgO in an aqueous fluid. This results in incongruent melting of brucite to periclase and liquid at higher pressure (reaction 2) (Fukui et al. 2005). However, from our in situ experiments we cannot determine the nature of the mobile phase (vapour, fluid, liquid; see Hermann et al. 2006 for a definition).

Brucite → Periclase + H_2O (1)

Brucite → Periclase + Liquid (2)

The in situ X-ray experiments conducted by Okada et al. (2002) confirmed periclase formation after reaction 1 at 3.6 GPa and 1050 °C. Unlike our findings, Okada et al. (2002) did not observe periclase crystallization associated with brucite breakdown at higher pressures (≥6.2 GPa), leading them to conclude that brucite completely melted. We favor an alternative interpretation mentioned by the authors themselves, which suggests that the size of periclase grains formed at high pressures in Okada et al. (2002) was too large to be detectable by EDXRD. In our study, we overcome this issue by using a lower amount of brucite in the starting material, oscillating the press, measuring at two different locations within the sample, and, in some experiments, employing two diffraction angles. These measures helped us overcome the aforementioned problem and obtain more accurate results.

In the magnesite + periclase + fluid stability field, the CO_2 content in the fluid will increase (isobarically) with increasing temperature, because the solubility of magnesite into the fluid increases until the liquidus is reached.

Melting of magnesite

We interpreted the disappearance of all reflections in the EDXRD measurements as the liquidus. With a fixed diffraction (2theta) angle, the absence of reflections in the diffraction pattern signifies that no crystal within the diffraction volume meets the reflection geometry. The growth of crystals during heating can hinder the accurate determination of a melting curve through EDXRD, as the crystals may become less likely to be oriented in the reflection geometry compared to a sample with numerous small crystals. To address this issue, we employed three strategies: (1) oscillating the press throughout the measurement, (2) conducting measurements at two positions within the sample when a phase change was

observed, and (3) using two detectors at different diffraction angles. Note that the last point only applies to experiments with a run number ≥153. The results from the measurements at different locations in the sample and the XRD patterns from the two detectors give conclusive results. It should be noted that the experimental set-up was not optimized for the observation of weak signals due to only partial melting. Therefore, diffuse scattering from the liquid phase was barely visible (Figure S2 in the supplementary information) and could not the utilized as a melting criterion.

Anhydrous-system

The melting point of magnesite has been well constrained and is depicted as solid black curve in Figure 4b, combining data from our anhydrous in situ experiment and previous quenched experiments (Irving and Wyllie 1975, Müller et al. 2017, Katsura and Ito 1990 and Shatskiy et al. 2018).

Earlier studies have revealed that the decomposition mechanism of magnesite is pressure dependent (Huang and Wyllie 1976; Irving and Wyllie 1975; Ellis and Wyllie 1979). Up to the *PT* conditions of an invariant point situated at 2.3 GPa and 1550 °C in the anhydrous system, magnesite undergoes incongruent decarbonation via the subsolidus reaction 3, resulting in the formation of periclase (Huang and Wyllie 1976; Irving and Wyllie 1975; Ellis and Wyllie 1979).

Magnesite → Periclase + CO_2 (3)

At pressures exceeding this invariant point, magnesite melts incongruently (reaction 4) (Ellis and Wyllie 1979).

Magnesite → Periclase + Liquid (4)

Recently, Sieber et al. (2022) demonstrated that incongruent melting of magnesite persists up to 6 and 9 GPa. Our in situ experiment confirm this finding, as periclase formation associated

with the breakdown of magnesite is detected by EDXRD. Thus, at 5.8 GPa and in the absence of a fluid, magnesite melts incongruently between 1725 and 1750 °C. These *PT* conditions are lower than those reported from falling sphere experiments for dry melting of magnesite (1750-1800 °C at 6 GPa; Müller et al. 2017). The requirement of relatively large melt proportions in experiments employing the falling sphere technique may explain the slight overestimation of the liquidus reported in Müller et al. (2017).

Hydrous system

Under hydrous conditions, magnesite is stable up to pressures and temperatures following the solid blue curve in Figure 4b. In the following we discuss the magnesite-out reactions from low (<2.3 GPa), to medium (2.3 GPa ≤ P <6.6 GPa) to high (≥6.6 GPa) pressures.

At 1.5 GPa (run 158), magnesite decomposes at ~1200 °C (Figure 4). This decomposition temperature is significantly higher compared to the earlier study conducted by Foustoukos and Mysen (2015). Foustoukos and Mysen (2015) performed in situ Raman measurements utilizing hydrothermal diamond-anvil cells and reported hydrous melting of magnesite coexisting with periclase to occur at ~850 °C and 1.5-2 GPa. The contrasting results might be attributed to the higher water content in Foustoukos and Mysen (2015) ($MgCO_3$+MgO to H_2O volumetric ratio of ~2:1). Oxygen fugacity may also affect the melting point (Lazar et al. 2014), although Foustoukos and Mysen (2015) did not observe a change in the melting temperature when utilizing Re-ReO_2 (oxidizing) and Ti-TiO_2 (reducing) as mineral redox buffer.

As mentioned above, an invariant point exists in the anhydrous system at 2.3 GPa and 1500 °C (Huang and Wyllie 1976; Irving and Wyllie 1975). However, we cannot determine

the presence and *PT* conditions of a brucite-absent invariant point in the hydrous system, as we are unable to distinguish between fluid and melt. If an invariant point does exist in the hydrous system, a change in the reaction slopes of reaction 3 and 4 would be expected. Note that reaction 3 (and also reaction 1) becomes divariant in the presence of a H_2O-CO_2 mixture (Ellis and Wyllie 1979; Walter et al. 1962). If we consider the pressure of 2.3 GPa determined for the anhydrous system, this invariant point would be located at ~1320 °C (labelled '(Br-I)' in Figure 4b) in the H_2O-bearing system. In such a scenario, magnesite would melt in the presence of a CO_2-H_2O fluid, resulting in periclase and carbonate-melt formation between 2.3 GPa and ~6.6 GPa. Alternatively, it is possible that magnesite breaks down to form periclase and a fluid up to ~6.6 GPa. In this interpretation, the point labelled Br-I in Figure 4b would not exist. Thermodynamic calculations do not provide conclusive presumptions in this regard. For instance, an assemblage of magnesite, periclase and a fluid is predicted at 1600 °C and 5 GPa. However, this cannot be confirmed by our data as, at these *PT* conditions, only periclase was observed in the EDXRD spectra (run 153). The thermodynamic predications also differ from the experimental results at higher pressures.

The liquidus temperature of hydrous magnesite at 6.6 GPa is between 1650 and 1675 °C (run 130). At the same pressure, with a slightly higher temperature of an additional 25 °C, periclase becomes unstable. Above ~7 GPa, the evaluation of the EDXRD data becomes somewhat ambiguous. This is due to the fact that, at elevated *PT* conditions, the positions of the main reflections from periclase and magnesite (e.g. periclase (200) with magnesite (113) and periclase (220) with magnesite (211)) almost overlap (Figure 3b). Additionally, the increased solubility of solids weakens the intensity of EDXRD reflections during heating.

Comparison between the anhydrous and hydrous system

For pressures up to ~6 GPa and coexisting with ~5 wt% of a H_2O-bearing fluid, the stability of magnesite is reduced by about ~100 °C compared to the anhydrous system. For example, ~6 GPa, the melting point of hydrous magnesite is determined to be between 1650 and 1675 °C, while the melting point of anhydrous magnesite falls within the range of 1725 to 1750 °C. This appears to be more reasonable than the smaller reduction of ~50 °C in the melting temperature obtained for hydromagnesite by Müller et al. (2017) from falling sphere experiments. The differences in fluid/magnesite ratio, temperature uncertainties, and/or potential (partial) fluid loss in the earlier experiments might contribute to this variation. Furthermore, by utilizing EDXRD, the onset of melting is indicated by rapid changes in the peak intensity of solids, enabling precise determination of the onset of melting (Andrault et al. 2006). In contrast, when employing the falling sphere technique in quenched experiments, the melting point needs to be determined through multiple experiments, resulting in a larger temperature gap between non-melting and melting experiments.

Figure 4

IMPLICATIONS

This experimental study demonstrates that magnesite remains stable in the presence of a hydrous fluid up to ~1200 °C at 1.6 GPa, ~1400 °C at 3.5 GPa and 1650-1675 °C between 6 to 9 GPa. As a result, it is unlikely for magnesite to undergo hydrous melting under typical temperature and pressure conditions observed in normal and hot subduction zones (Syracuse et al. 2010). These findings carry significant implications. For example, magnesite can persist within the subducting slab and be transported to sub-arc depths, even in the presence of fluids containing H_2O released during dehydration reactions from hydrous phases during

subduction. Importantly, these results and conclusions differ from the previous findings of Foustoukos and Mysen (2015), who suggested that magnesite melts in the presence of a fluid and periclase below ~3 GPa. The discrepancy between the conclusions of these two studies emphasizes the importance of further investigating the H_2O-carbonate system under various *PT* conditions and fluid/solid ratios.

CONCLUSION

Through synchrotron in situ EDXRD experiments and quenched experiments utilizing the falling sphere technique, this study validates the published dehydration and melting curves of brucite and elucidates the disintegration of magnesite in the presence of periclase and an H_2O-bearing fluid within the pressure range of 1 GPa to 12 GPa.

Consistent with previous studies, our findings demonstrate that brucite undergoes incongruent dehydration, resulting in the formation of periclase and an aqueous fluid up to 4 GPa and around 1130 °C. As pressure increases to 12 GPa, brucite decomposes, leading to the generation of periclase and a supercritical fluid / liquid at similar temperatures.

In the presence of periclase and an aqueous fluid, we have observed that magnesite remains stable up to temperatures such as approximately 1200 °C at 1.6 GPa and around 1400 °C at 3.5 GPa. Between 6 GPa and 9 GPa, magnesite coexists with periclase and a fluid/liquid up to temperatures ranging from 1650 to 1675 °C. The addition of approximately 5 wt% of H_2O to the system lowers the stability of magnesite by approximately 100 °C for pressures below 6.5 GPa. For pressures exceeding 6.5 GPa, the liquidus temperatures of the anhydrous and hydrous systems diverge as pressure increases.

Based on these findings, we can conclude that hydrous melting of magnesite is improbable under the typical temperature and pressure conditions observed in both normal and hot

subduction zones. Consequently, magnesite has the potential to be transported within the subducting slab to sub arc depths and beyond.

ACKNOWLEDGMENTS

We are grateful to A. Ebert (GFZ), C. Günter (Uni Potsdam), L. Koldeweyh (Uni Potsdam), A. Schreiber (GFZ), S. Bhat (DESY) and C. Lathe (GFZ) for their assistance in experimental and analytical work. We acknowledge constructive comments and suggestion from O. Lord and S. Dorfman. We thank S. Dorfman for editorial handing of the paper.

This study was funded by the DFG funded research group FOR2125 CarboPaT under the grant number KO1260/19-1. We acknowledge DESY (Hamburg, Germany), a member of the Helmholtz Association HGF, for the provision of experimental facilities. Parts of this research were carried out at beamline P61B (Proposal I-20200568 and I-20210429) with the support from the Federal Ministry of Education and Research, Germany (BMBF, grants no.: 05K16WC2 & 05K13WC2). The authors also acknowledge the scientific exchange and support of the Centre for Molecular Water science (CMWS).

REFERENCES CITED

Andrault, D., Morard, G., Bolfan-Casanova, N., Ohtaka, O., Fukui, H., Arima, H., Guignot, N., Funakoshi, K., Lazor, P., and Mezouar, M. (2006) Study of partial melting at high-pressure using in situ X-ray diffraction. High Pressure Research, 26 (3), 267–276, DOI: 10.1080/08957950600897013.

Connolly, J.A.D. (2005) Computation of phase equilibria by linear programming: A tool for geodynamic modeling and its application to subduction zone decarbonation. Earth and Planetary Science Letters, 236 (1-2), 524–541, DOI: 10.1016/j.epsl.2005.04.033 (English).

Dasgupta, R., and Hirschmann, M.M. (2006) Melting in the Earth's deep upper mantle caused by carbon dioxide. Nature, 440 (7084), 659–662, DOI: 10.1038/nature04612.

Dasgupta, R., Hirschmann, M.M., and Withers, A.C. (2004) Deep global cycling of carbon constrained by the solidus of anhydrous, carbonated eclogite under upper mantle conditions. Earth and Planetary Science Letters, 227 (1-2), 73–85, DOI: 10.1016/j.epsl.2004.08.004.

Della Roy, M., and Roy, R. (1957) A re-determination of equilibria in the system MgO-H_2O and comments on earlier work. American Journal of Science, 255 (8), 574–583, DOI: 10.2475/ajs.255.8.574.

Deon, F., Koch-Müller, M., Rhede, D., and Wirth, R. (2011) Water and Iron effect on the P-T-x coordinates of the 410-km discontinuity in the Earth upper mantle. Contributions to Mineralogy and Petrology, 161 (4), 653–666, DOI: 10.1007/s00410-010-0555-6.

Ellis, D.E., and Wyllie, P.J. (1979) Carbonation, hydration, and melting relations in the system MgO-H2O-CO2 at pressures up to 100 kbar. American Mineralogist, 64 (1-2), 32–40, DOI: 10.1007/BF00372117.

Falloon, T.J., and Green, D.H. (1989) The solidus of carbonated, fertile peridotite. Earth and Planetary Science Letters, 94 (3), 364–370, DOI: 10.1016/0012-821X(89)90153-2.

Farla, R., Bhat, S., Sonntag, S., Chanyshev, A., Ma, S., Ishii, T., Liu, Z., Neri, A., Nishiyama, N., Faria, G.A., Wroblewski, T., Schulte-Schrepping, H., Drube, W., Seeck, O., and Katsura, T. (2022) Extreme conditions research using the large-volume press at the P61B endstation, PETRA III. Journal of synchrotron radiation, 29 (2), 409–423, DOI: 10.1107/S1600577522001047.

Foustoukos, D.I., and Mysen, B.O. (2015) The structure of water-saturated carbonate melts†. American Mineralogist, 100 (1), 35–46, DOI: 10.2138/am-2015-4856.

Fukui, H., Inoue, T., Yasui, T., Katsura, T., Funakoshi, K.-I., and Ohtaka, O. (2005) Decomposition of brucite up to 20 GPa: evidence for high MgO-solubility in the liquid phase. Eur J Mineral, 17 (2), 261–267, DOI: 10.1127/0935-1221/2005/0017-0261.

Galvez, M.E., and Pubellier, M. (2019) How Do Subduction Zones Regulate the Carbon Cycle? In B.N. Orcutt, I. Daniel, and R. Dasgupta, Eds., Deep Carbon: past to present, p. 276–312. Cambridge University Press.

Green, D.H., Hibberson, W.O., Rosenthal, A., Kovács, I., Yaxley, G.M., Falloon, T.J., and Brink, F. (2014) Experimental Study of the Influence of Water on Melting and Phase Assemblages in the Upper Mantle. Journal of Petrology, 55 (10), 2067–2096, DOI: 10.1093/petrology/egu050.

Hermann, J., Spandler, C., Hack, A., and Korsakov, A.V. (2006) Aqueous fluids and hydrous melts in high-pressure and ultra-high pressure rocks: implications for element transfer in subduction zones. Lithos, 92 (3-4), 399–417.

Hernlund, J., Leinenweber, K., Locke, D., and Tyburczy, J.A. (2006) A numerical model for steady-state temperature distributions in solid-medium high-pressure cell assemblies. American Mineralogist, 91 (2-3), 295–305, DOI: 10.2138/am.2006.1938.

Holland, T.J.B., and Powell, R. (1998) An internally consistent thermodynamic data set for phases of petrological interest. Journal of Metamorphic Geology, 16 (3), 309–343, DOI: 10.1111/j.1525-1314.1998.00140.x (English).

Holland, T.J.B., and Powell, R. (2011) An improved and extended internally consistent thermodynamic dataset for phases of petrological interest, involving a new equation of state for solids. Journal of Metamorphic Geology, 29 (3), 333–383, DOI: 10.1111/j.1525-1314.2010.00923.x (English).

Huang, W.-L., and Wyllie, P.J. (1976) Melting relationships in the systems CaO-CO2 and MgO-CO2 to 33 kilobars. Geochimica et Cosmochimica Acta, 40 (2), 129–132, DOI: 10.1016/0016-7037(76)90169-1.

Inoue, T. (1994) Effect of water on melting phase relations and melt composition in the system Mg2SiO4-MgSiO3-H2O up to 15 GPa. Physics of the Earth and Planetary Interiors, 85 (3), 237–263, DOI: 10.1016/0031-9201(94)90116-3.

Irving, A.J., and Wyllie, P.J. (1975) Subsolidus and melting relationships for calcite, magnesite and the join CaCO3-MgCO3 36 kb. Geochimica et Cosmochimica Acta, 39 (1), 35–53, DOI: 10.1016/0016-7037(75)90183-0.

Johnson, M.C., and Walker, D. (1993) Brucite [MG(OH)2] dehydration and the molar volume of H2O to 15 GPa. American Mineralogist, 78 (3-4), 271–284.

Katsura, T., and Ito, E. (1990) Melting and subsolidus phase relations in the MgSiO3MgCO3 system at high pressures: implications to evolution of the Earth's atmosphere. Earth and Planetary Science Letters, 99 (1-2), 110–117, DOI: 10.1016/0012-821x(90)90074-8.

Kelemen, P.B., and Manning, C.E. (2015) Reevaluating carbon fluxes in subduction zones, what goes down, mostly comes up. Proc Natl Acad Sci U S A, 112 (30), E3997-4006, DOI: 10.1073/pnas.1507889112.

Lazar, C., Zhang, C., Manning, C.E., and Mysen, B.O. (2014) Redox effects on calcite-portlandite-fluid equilibria at forearc conditions: Carbon mobility, methanogenesis, and reduction melting of calcite. American Mineralogist, 99 (8-9), 1604–1615, DOI: 10.2138/am.2014.4696.

Müller, J., Koch-Müller, M., Rhede, D., Wilke, F.D.H., and Wirth, R. (2017) Melting relations in the system CaCO3-MgCO3 at 6 GPa. American Mineralogist, 102 (12), 2440–2449, DOI: 10.2138/am-2017-5831.

Okada, T., Utsumi, W., and Shimomura, O. (2002) In situ x-ray observations of the diamond formation process in the C-H2O-MgO system. Journal of Physics: Condensed Matter, 14 (44), 11331–11335, DOI: 10.1088/0953-8984/14/44/477.

Orcutt, B.N., Daniel, I., and Dasgupta, R., Eds. (2019) Deep Carbon: past to present Cambridge University Press.

Poli, S. (2015) Carbon mobilized at shallow depths in subduction zones by carbonatitic liquids. Nature Geoscience, 8 (8), 633–636, DOI: 10.1038/ngeo2464.

Poli, S., Franzolin, E., Fumagalli, P., and Crottini, A. (2009) The transport of carbon and hydrogen in subducted oceanic crust: An experimental study to 5 GPa. Earth and Planetary Science Letters, 278 (3-4), 350–360, DOI: 10.1016/j.epsl.2008.12.022.

Shatskiy, A.F., Litasov, K.D., and Palyanov, Y.N. (2015) Phase relations in carbonate systems at pressures and temperatures of lithospheric mantle: review of experimental data. Russian Geology and Geophysics, 56 (1-2), 113–142, DOI: 10.1016/j.rgg.2015.01.007.

Shatskiy, A., Litasov, K.D., Sharygin, I.S., Egonin, I.A., Mironov, A.M., Palyanov, Y.N., and Ohtani, E. (2016) The system Na2CO3–CaCO3–MgCO3at 6 GPa and 900–1250°C and its relation to the partial melting of carbonated mantle. High Pressure Research, 36 (1), 23–41, DOI: 10.1080/08957959.2015.1135916.

Shatskiy, A., Podborodnikov, I.V., Arefiev, A.V., Minin, D.A., Chanyshev, A.D., and Litasov, K.D. (2018) Revision of the CaCO3–MgCO3 phase diagram at 3 and 6 GPa. American Mineralogist, 103 (3), 441–452, DOI: 10.2138/am-2018-6277.

Shen, J., Li, S.-G., Wang, S.-J., Teng, F.-Z., Li, Q.-L., and Liu, Y.-S. (2018) Subducted Mg-rich carbonates into the deep mantle wedge. Earth and Planetary Science Letters, 503, 118–130, DOI: 10.1016/j.epsl.2018.09.011.

Sieber, M.J., Wilke, F., and Koch-Müller, M. (2020) Partition coefficients of trace elements between carbonates and melt and suprasolidus phase relation of Ca-Mg-carbonates at 6 GPa. American Mineralogist, 105 (6), 922–931, DOI: 10.2138/am-2020-7098.

Sieber, M.J., Wilke, M., Appelt, O., Oelze, M., and Koch-Müller, M. (2022) Melting relations of Ca-Mg-carbonates and trace element signature of carbonate melts up to 9 GPa as proxy for melting of carbonated mantle lithologies. European Journal of Mineralogy, 34, 411–424, DOI: 10.5194/ejm-34-411-2022.

Syracuse, E.M., van Keken, P.E., and Abers, G.A. (2010) The global range of subduction zone thermal models. Physics of the Earth and Planetary Interiors, 183 (1-2), 73–90, DOI: 10.1016/j.pepi.2010.02.004.

Tange, Y., Nishihara, Y., and Tsuchiya, T. (2009) Unified analyses for P-V-T equation of state of MgO: A solution for pressure-scale problems in high P-T experiments. Journal of Geophysical Research: Solid Earth, 114 (B3), DOI: 10.1029/2008JB005813.

Walter, L.S., Wyllie, P.J., and Tuttle, O.F. (1962) The System MgO-CO2-H2O at High Pressures and Temperatures1. Journal of Petrology, 3 (1), 49–64, DOI: 10.1093/petrology/3.1.49.

Wyllie, P.J., and Tuttle, O.F. (1960) The System CaO-CO2-H2O and the Origin of Carbonatites. Journal of Petrology, 1 (1), 1–46.

Yamada, A., Inoue, T., Urakawa, S., Funakoshi, K.-I., Funamori, N., Kikegawa, T., Ohfuji, H., and Irifune, T. (2007) In situ X-ray experiment on the structure of hydrous Mg-silicate melt under high pressure and high temperature. Geophys Res Lett, 34 (10), 1–5, DOI: 10.1029/2006GL028823.

TABLES CAPTION

Table 1: Overview of the performed falling sphere and in situ experiments.

FIGURE CAPTION

Figure 1: Technical drawing of the 14/8 assembly used for in situ experiments (viewing direction is in line with X-ray beam as indicated).

Figure 2: (a + b) backscatter electron (BSE) images of polished samples from falling sphere experiments. (a) Hour-glass texture with needle-shaped brucite crystals and small periclase grains in hot areas of the capsule and larger grained periclase and magnesite in colder areas of the capsule. This texture reports breakdown of brucite without hydrous melting of magnesite (details in text) (b) partial melting is evidenced texturally but the Pt-sphere remained at the top of the capsule; (c-f) recovered samples from in situ experiments (c) overview of the samples surrounded by the diamond cylinder, which is broken in half while extracting the sample from the assembly; (d) close up view of a sample from in situ experiments. Abbreviations: Mgs: magnesite; Per: periclase; Pt: Pt-sphere

Figure 3: Selected EDXRD spectra during heating cycle; (a) run 153 at 4.9 GPa where periclase was stable up to the highest investigated temperature, 2theta angle is 4.9834°; (b) run 132 at 8.3 GPa indicating hydrous melting of magnesite, 2theta angle is 5.1670°. (c) enlargement of EDXRD spectra from the three highest temperatures shown in (b). Boxes mark the appearance and disappearance of mineral reflection associated with a change in the stable mineral assemblage.

Figure 4: (a) Phase assemblages as observed by in situ EDXRD and *PT* conditions of falling sphere experiments; (b) Interpreted reaction curves (sketched by eye) and stable mineral phases in comparison to literature data (references in text). (1) Mgs + Per = melt; (2) Mgs = melt

SUPPLEMENTARY INFORMATION

Thermodynamic calculations

For comparison between the experimental results and thermodynamic predictions, phase diagrams were calculated using the bulk MgO-CO_2-H_2O composition of our starting material. In the modelling a gridded minimization strategy and linear programming for optimization (Connolly 2005) was applied with Perple_X. The thermodynamic dataset from Holland and Powell (1998) and Holland and Powell (2011) were used.

Figure S1: Good correlation of the pressure obtained from EDXRD measurements of periclase from the sample (inside the diamond cylinder) to the pressure of the assemblage (outside the diamond cylinder) for temperature ≥1000 °C. Symbols in grey point to experiments that were excluded from the data interpretation due to loss of volatiles under high *PT*.

Figure S2: shows normalized intensities as a function of the scattering vector (*Q*) for EDXRD measurements of run 132 at different temperatures. The intensities are normalized to a spectrum acquired at high *PT* of the same experiment where the starting material (magnesite + brucite) was still stable. A weak diffuse scattering signal of the liquid can be seen at 1690 °C. This confirms the presence of melt independent of our main melting criterion (see text). However, the results shown here are not unambiguous, because the experimental design was not optimized for this approach.

Figure S3: For better comparison between the experimental data and our interpretation of phase boundaries, we show here an overlap of panel a and b of Figure 4 from the main manuscript.

This is the peer-reviewed, final accepted version for American Mineralogist, published by the Mineralogical Society of America.
The published version is subject to change. Cite as Authors (Year) Title. American Mineralogist, in press.
DOI: https://doi.org/10.2138/am-2023-8982. http://www.minsocam.org/

Figure 1

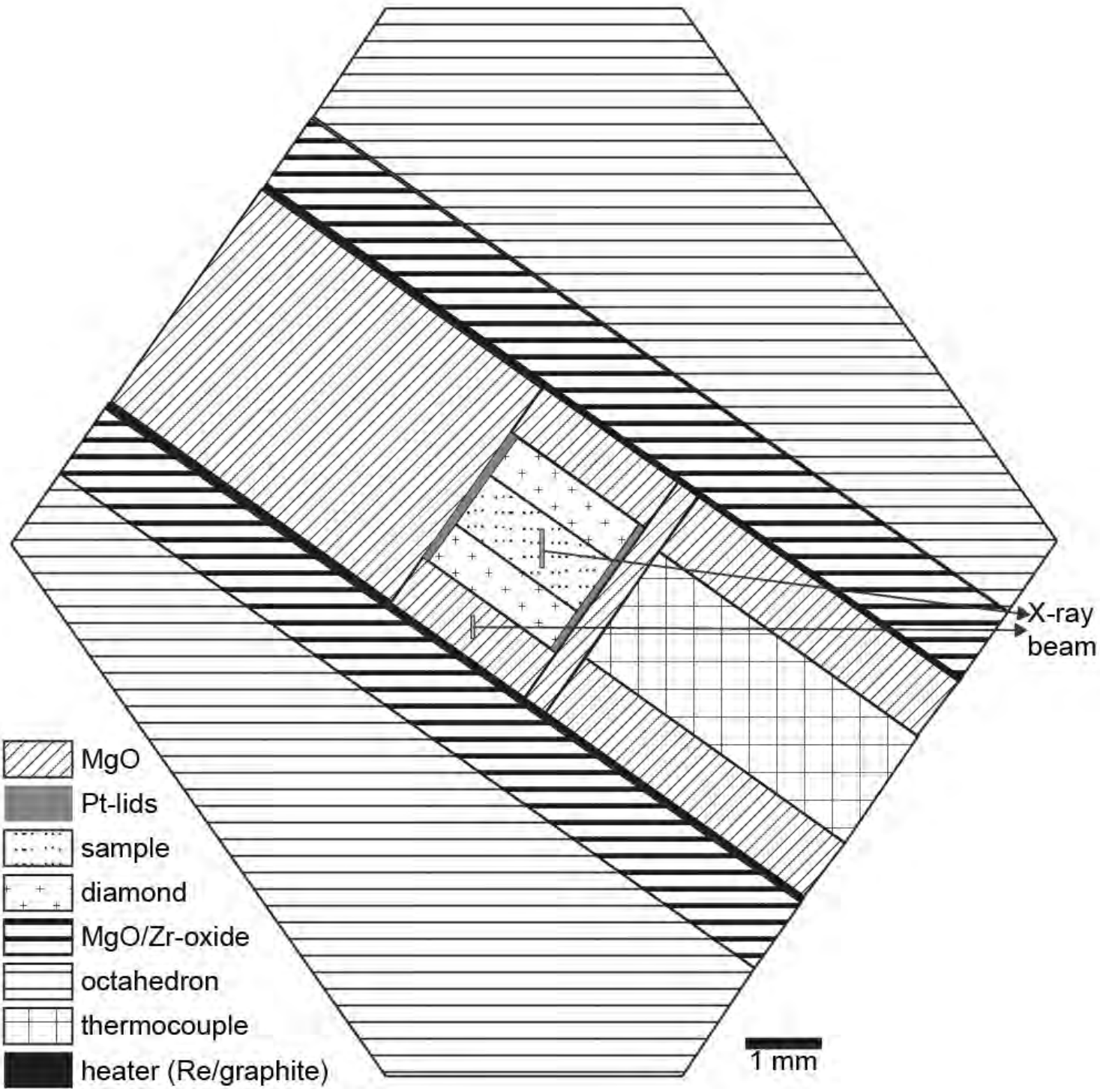

This is the peer-reviewed, final accepted version for American Mineralogist, published by the Mineralogical Society of America.
The published version is subject to change. Cite as Authors (Year) Title. American Mineralogist, in press.
DOI: https://doi.org/10.2138/am-2023-8982. http://www.minsocam.org/

Figure 2

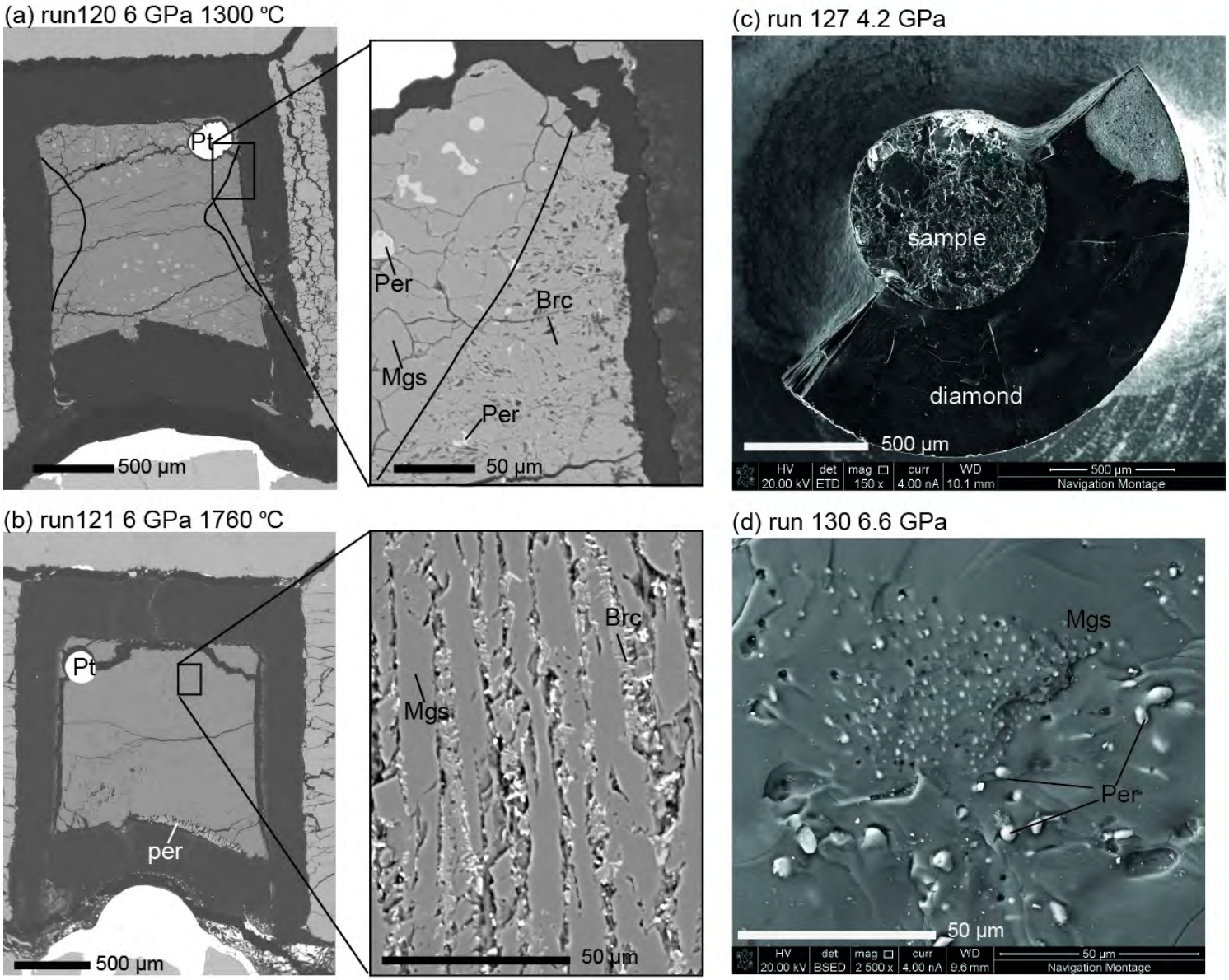

This is the peer-reviewed, final accepted version for American Mineralogist, published by the Mineralogical Society of America.
The published version is subject to change. Cite as Authors (Year) Title. American Mineralogist, in press.
DOI: https://doi.org/10.2138/am-2023-8982. http://www.minsocam.org/

Figure3a

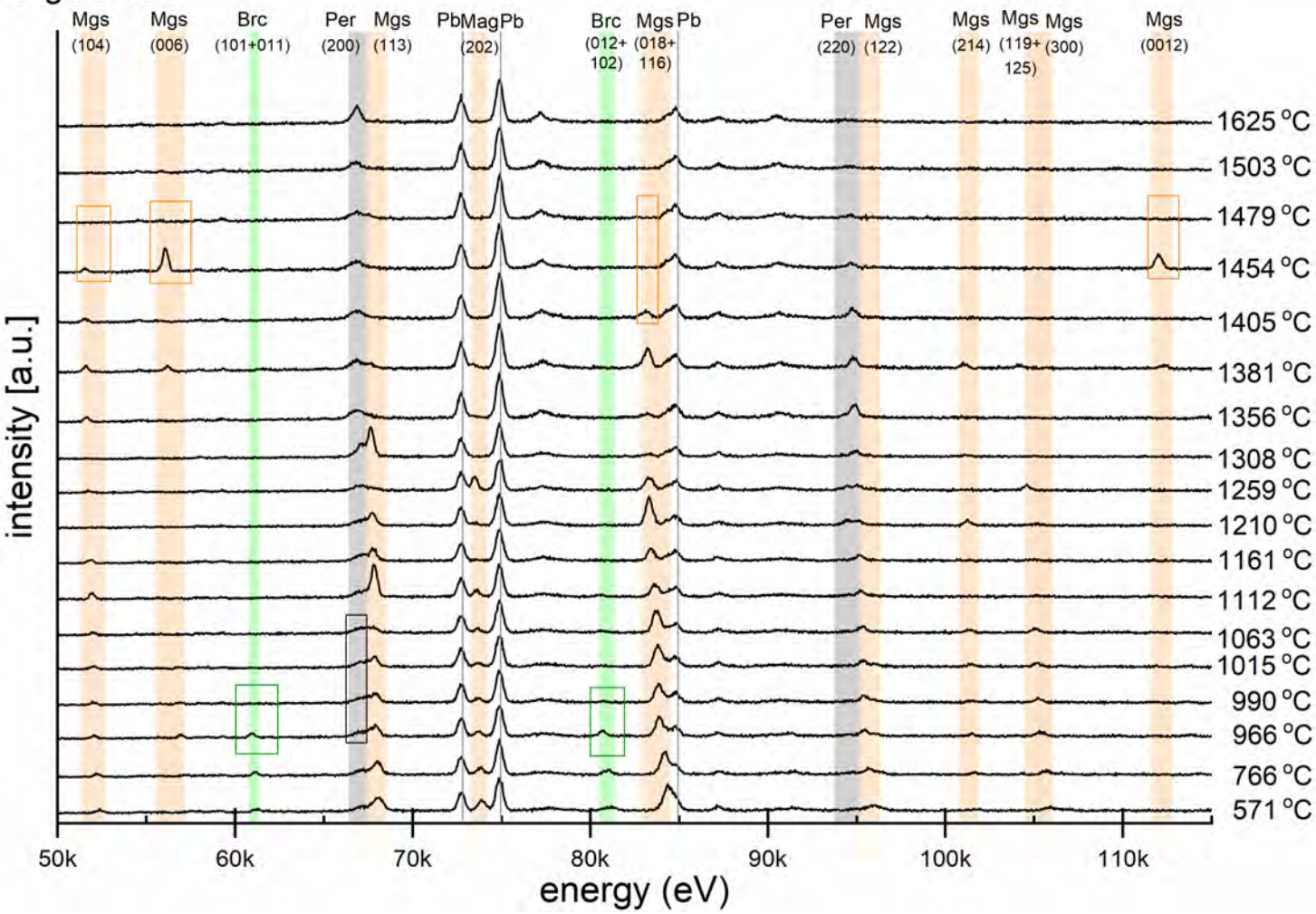

This is the peer-reviewed, final accepted version for American Mineralogist, published by the Mineralogical Society of America.
The published version is subject to change. Cite as Authors (Year) Title. American Mineralogist, in press.
DOI: https://doi.org/10.2138/am-2023-8982. http://www.minsocam.org/

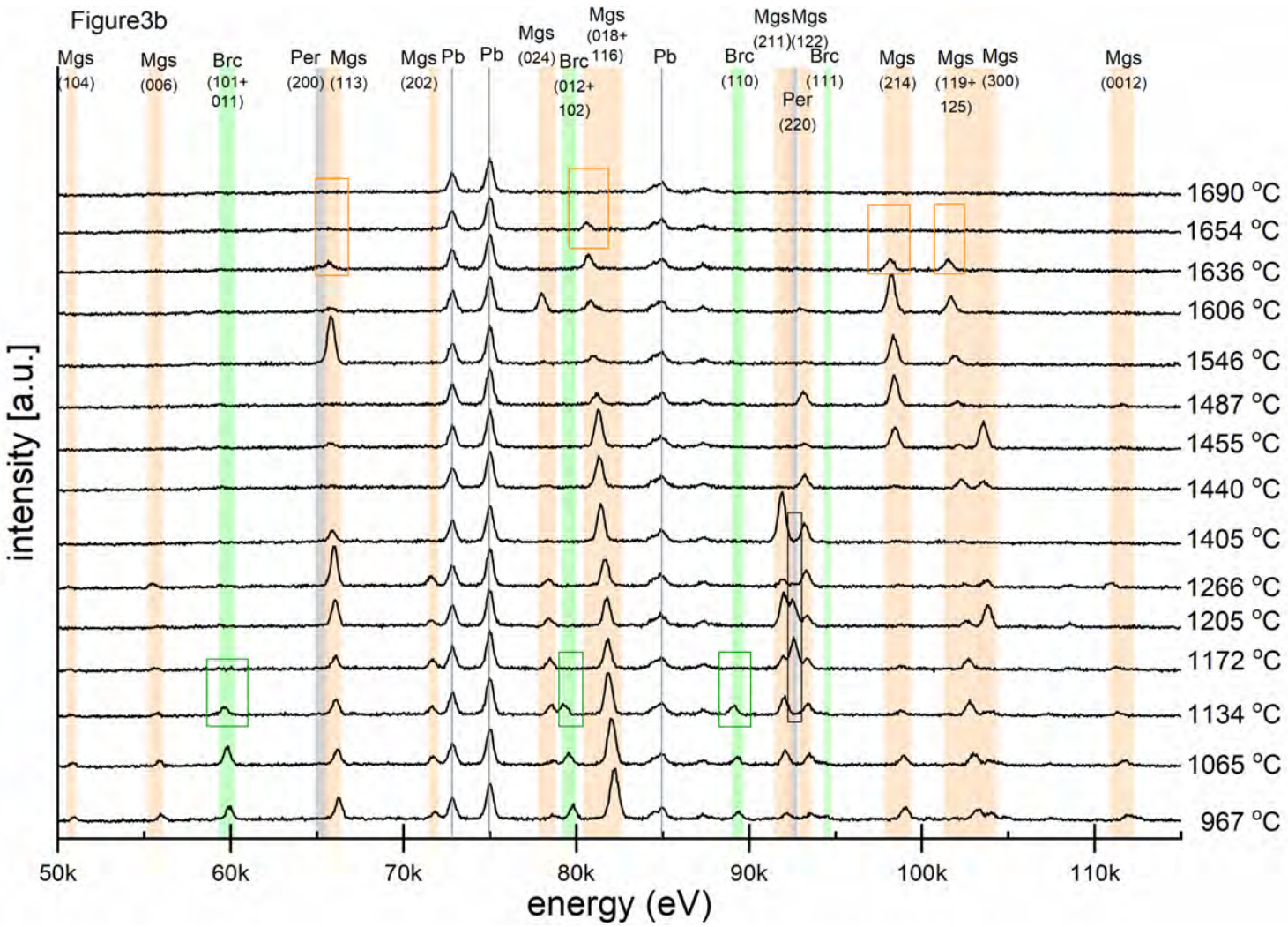

This is the peer-reviewed, final accepted version for American Mineralogist, published by the Mineralogical Society of America.
The published version is subject to change. Cite as Authors (Year) Title. American Mineralogist, in press.
DOI: https://doi.org/10.2138/am-2023-8982. http://www.minsocam.org/

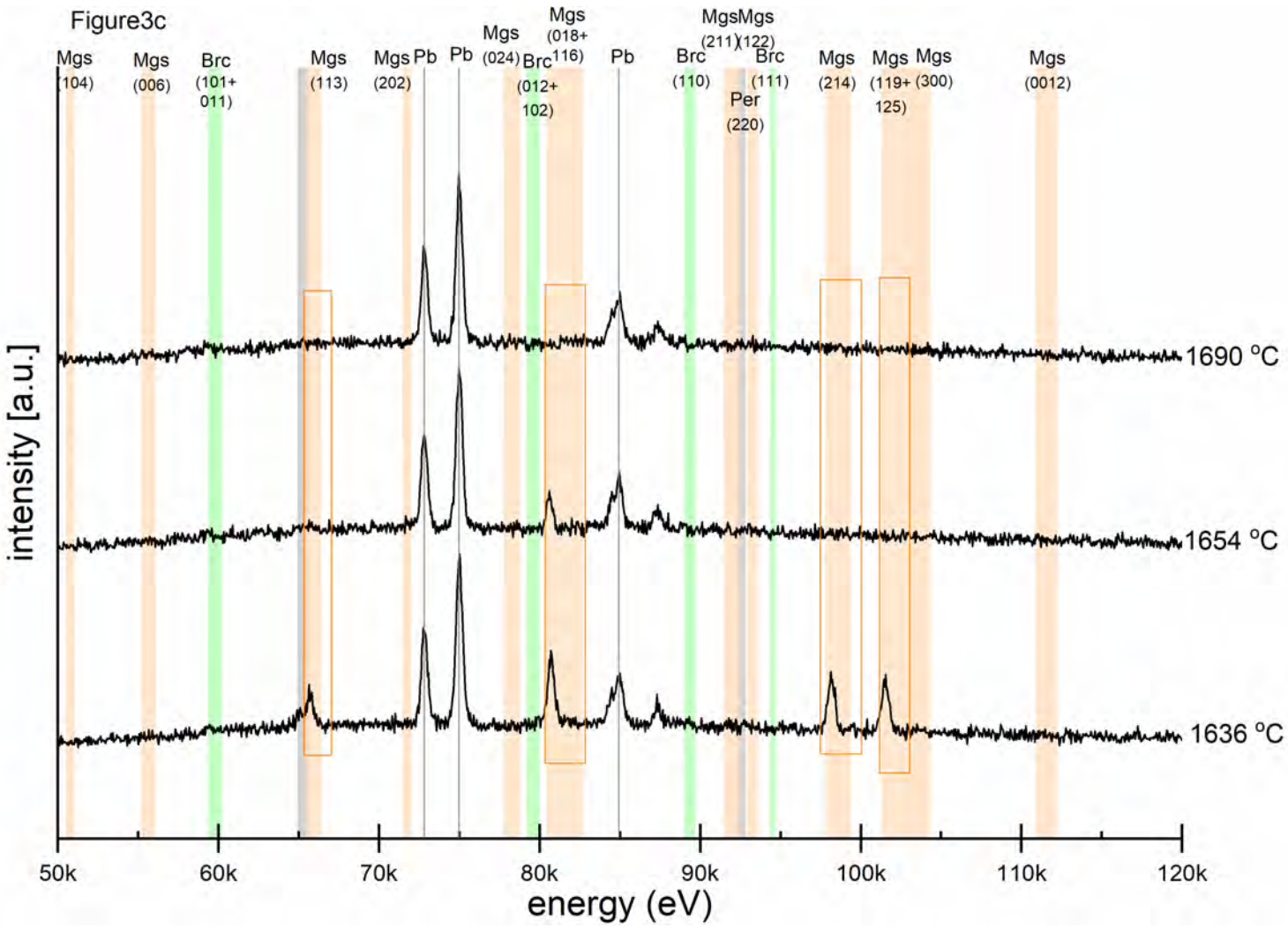

This is the peer-reviewed, final accepted version for American Mineralogist, published by the Mineralogical Society of America.
The published version is subject to change. Cite as Authors (Year) Title. American Mineralogist, in press.
DOI: https://doi.org/10.2138/am-2023-8982. http://www.minsocam.org/

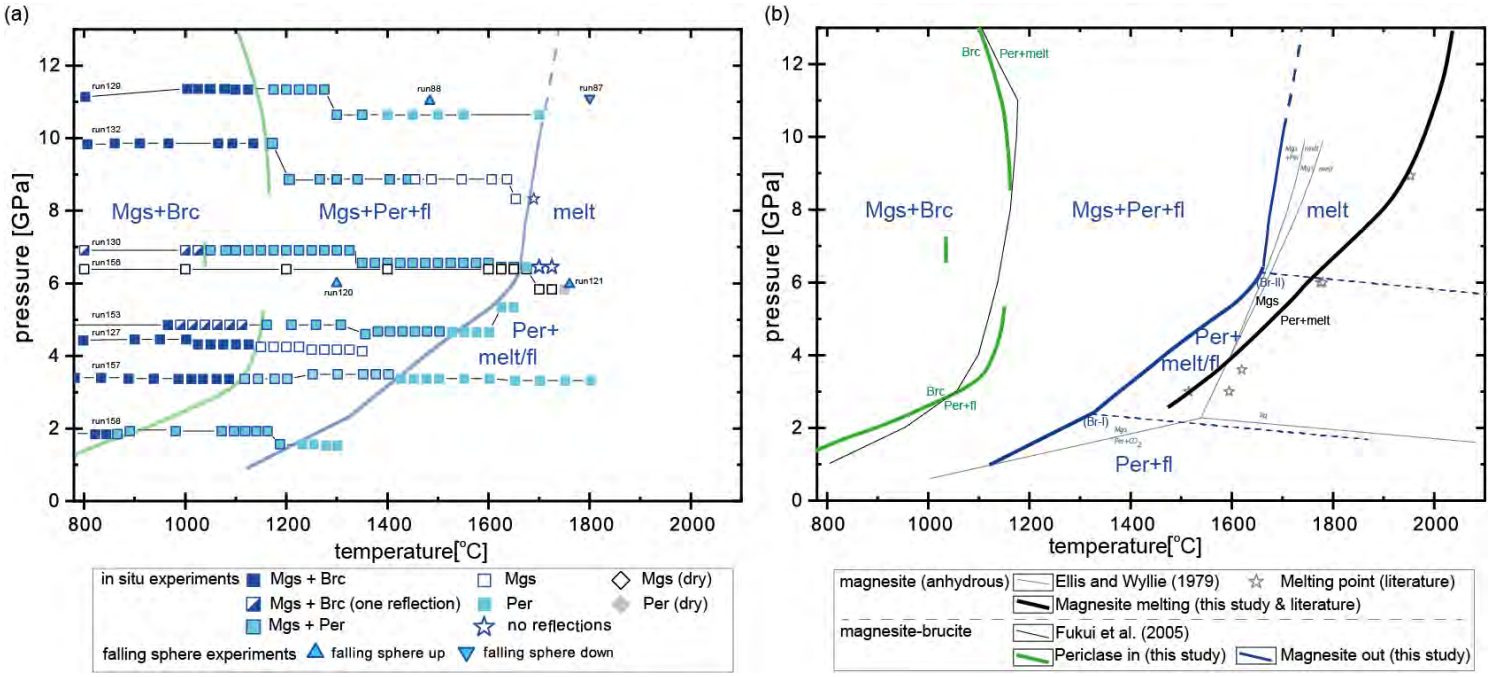

run number	start material	method	multi-anvil press	heater
87	magnesite-brucite	falling-sphere	LVP @ P61.B	Re
88	magnesite-brucite	falling-sphere	LVP @ P61.B	Re
120	magnesite-brucite	falling-sphere	LVP @ GFZ	graphite
121	magnesite-brucite	falling-sphere	LVP @ GFZ	graphite
127	magnesite-brucite	in situ EDXRD	LVP @ P61.B	graphite
128	magnesite-brucite	in situ EDXRD	LVP @ P61.B	Re
129	magnesite-brucite	in situ EDXRD	LVP @ P61.B	Re
130	magnesite-brucite	in situ EDXRD	LVP @ P61.B	graphite
131	magnesite-brucite	in situ EDXRD	LVP @ P61.B	graphite
132	magnesite-brucite	in situ EDXRD	LVP @ P61.B	graphite
153	magnesite-brucite	in situ EDXRD	LVP @ P61.B	graphite
156	magnesite	in situ EDXRD	LVP @ P61.B	graphite
157	magnesite-brucite	in situ EDXRD	LVP @ P61.B	graphite
158	magnesite-brucite	in situ EDXRD	LVP @ P61.B	graphite

* for heating cycle and temperatures ≥1000 ℃
** T (temperature) uncertainty has been calculated to be ~30 ℃

RT: room temperature; LVP: Large Volume Press; P61.B: beamline at the Deutsches Ele

OH* : a fine grained phase containing OH was observed (OH-band detected by Raman s

capsule	thermocouple	T max **	*P* oil	*P* press	*P* MgO assemblage			post run assembly
						mean*	SD*	
		℃	bar	GPa	GPa	GPa	GPa	
Pt	Type C	1800	260	10.8				Mgs, Per, Brc
Pt	failed	~1485	260	10.8				Mgs, Per, Brc
graphite	Type C	1300		6				Mgs, Per, Brc
graphite	Type C	1760		6				Mgs, Per, Brc
diamond	Type C	RT	85		5.1			Mgs, Per, Brc, graphite
		1025	100			3.8	0.3	
		1350	120			4.2	0.1	
diamond	Type C	RT	255		12.3			Mgs, Per
		1500	255			10.8	0.7	
diamond	Type C	600	255		10.1			Mgs, Per, OH*
		1700	300			11.1	0.4	
diamond	Type C	RT	150		8.6			Mgs, Per, OH*
		1725	150			6.6	0.2	
diamond	Type C	RT	70		3.3			Mgs, Per
		1300	90		5.6	4.1	0.2	
diamond	failed	RT	200		10.3			Mgs, Per, OH*
		1734	200			8.3	0.6	
diamond	failed	RT	135		6.6			Mgs, Per, OH*
		1650	135			4.9	0.4	
diamond	Type C	RT	150		8.9			Mgs, Per
		1750	150			6.1	0.4	
diamond	failed	RT	100		5.1			Mgs, Per, Br
		1800	100			3.4	0.1	
diamond	failed	RT	50		1.9			Mgs, Per, Br
		1300	50			1.5	0.03	

ektronen-Synchrotron; GFZ: German Research Centre for Geosciences

spectroscopy).

This is the peer-reviewed, final accepted version for American Mineralogist, published by the Mineralogical Society of America.
The published version is subject to change. Cite as Authors (Year) Title. American Mineralogist, in press.
DOI: https://doi.org/10.2138/am-2023-8982. http://www.minsocam.org/

position of Pt-sphere
bottom
top
top
top